Liquid Crystals
Publication details, including instructions for authors and subscription information:
http://www.informaworld.com/smpp/title~content=t713926090

Computer simulation of elongated bipolar nematic droplets 1. External field aligned parallel to the droplet axis of symmetry

Philip K. Chan

Online publication date: 06 August 2010

To cite this Article Chan, Philip K.(1999) 'Computer simulation of elongated bipolar nematic droplets 1. External field aligned parallel to the droplet axis of symmetry', Liquid Crystals, 26: 12, 1777 — 1786
To link to this Article: DOI: 10.1080/026782999203409
URL: http://dx.doi.org/10.1080/026782999203409

LIQUID CRYSTALS, 1999, VOL. 26, NO. 12, 1777–1786

Computer simulation of elongated bipolar nematic droplets 1. External field aligned parallel to the droplet axis of symmetry

PHILIP K. CHAN

School of Chemical Engineering, Ryerson Polytechnic University,
350 Victoria Street, Toronto, Ontario, Canada M5B 2K3;
e-mail: p4chan@acs.ryerson.ca

(*Received 17 May 1999; accepted 1 July 1999*)

The magnetically-induced transient nematic director reorientation dynamics, confined in elongated bipolar droplets, is studied in this paper. Numerical results are obtained by solving the Leslie–Ericksen continuum theory in ellipses. The aspect ratio is varied to determine the effect of droplet shape on director reorientation dynamics. The magnetic field is restricted to the droplet axis of symmetry direction, which has not yet been studied but is fundamentally important in polymer dispersed liquid crystal (PDLC) film operation. The numerical results replicate frequently-reported experimental observations on the performance of PDLC films. These observations include the familiar exponential increases followed by saturation in light transmittance as the external applied field increases and the exponential increase (decrease) followed by saturation as time increases in the on- (off-) state. In addition, the experimental observation that switching field strength increases while decay time decreases as the droplet becomes more elongated, are also exhibited by the numerical results.

1. Introduction

Research on bipolar nematic droplets began 30 years ago with the theoretical work of Dubois-Violette and Parodi [1], which was then followed by the experimental work of Candau *et al.* [2]. The director configuration of a nematic bipolar droplet is due to the director being anchored tangentially to the surface; this results, after the minimization of the bulk elastic free energy, in two point defects located at each end of the axis of symmetry. Research has intensified in the last decade on these droplets [3–10], because of their use in polymer dispersed liquid crystal (PDLC) films [11–21].

PDLC films consist of micron-size liquid crystalline droplets dispersed uniformly in a solid polymer matrix; they are used in practical display applications such as switchable windows, billboards and flat panel television screens. The principle idea behind PDLC film operation is very simple: the film is opaque in its natural state but becomes transparent when an electric field of sufficient strength is applied normally to it. For nematics with positive dielectric anisotropy, this electro-optical response from opaque to transparent is due to the director reorienting within the bipolar droplets to align with the electric field direction. It has been noted that the magneto-optical response of PDLC films shares the same characteristic properties as the electro-optical response described above [13].

Depending on the film fabrication procedure, the droplet shape can range from spherical to elongated. Fabrication procedures include the thermal-induced, polymerization-induced and shear-induced phase separation methods and the emulsification method [3, 4, 11, 12, 15–21]. In addition, the droplet axis of symmetry can be oriented anywhere from along the normal to the film plane to within the film plane. The magneto-optical and electro-optical responses, such as the switching field strength (which is defined as the field strength required to obtain 90% light transmittance) and decay time (which is defined as the time required for the film to return to 10% light transmittance after the external field has been removed), depend on the droplet shape. It is desirable to design a PDLC film that requires a low switching field strength, has a low decay time, and has good light contrast between the on- and off-states. It has been determined experimentally that switching field strength is lower for a spherical droplet than for an elongated droplet, while the decay time is lower for an elongated droplet than for a spherical droplet [3].

Presently, the literature on bipolar nematic droplets contains some dynamic experimental [3, 5, 7] and steady-state numerical work [6, 8, 9], and, to the author's knowledge, only one dynamic numerical study which is on spherical droplets [10]. Because of the importance

Journal of Liquid Crystals ISSN 0267-8292 print/ISSN 1366-5855 online © 1999 Taylor & Francis Ltd
http://www.tandf.co.uk/JNLS/lct.htm
http://www.taylorandfrancis.com/JNLS/lct.htm

of droplet shape on the magneto-optical and electro-optical responses of PDLC films, this paper extends the dynamical study by Chan and Rey [10] to elongated droplets. The objective of this paper is to present results from a two-dimensional numerical study on the transient director configuration in elongated bipolar nematic droplets when a magnetic field is applied parallel to the droplet axis of symmetry. This represents the extreme case where the droplet axis of symmetry is normal to the film plane; it is believed that this important scenario has not yet been studied. The model incorporates the Leslie–Ericksen continuum theory for bulk director reorientation dynamics and the Frank continuum theory for the elastic free energy density [22]. The rest of this paper is organized as follows. The governing equations, auxiliary conditions, and the method of solution are given in § 2. The numerical results are presented, discussed and contrasted with published experimental results in § 3. Conclusions are given in § 4.

2. Problem formulation and numerical methods

In this section background theory required for this paper is presented briefly; model development is then given and this is followed by a description of the numerical method of solution used to solve the model.

2.1. *Theory*

According to the Leslie–Ericksen theory [22], director reorientation is governed by the following torque balance equation written in Cartesian tensorial notation:

$$\mathbf{\Gamma}_e + \mathbf{\Gamma}_v + \mathbf{\Gamma}_m = 0 \tag{1}$$

where the three terms on the left hand side denote the elastic torque, viscous torque, and magnetic torque on the director per unit volume, respectively. Their constitutive equations are as follows:

$$\mathbf{\Gamma}_e = -\mathbf{n} \times \frac{\delta f_d}{\delta \mathbf{n}} \tag{2a}$$

$$\mathbf{\Gamma}_v = -\mathbf{n} \times (\gamma_1 \mathbf{N} + \gamma_2 \mathbf{A} \cdot \mathbf{n}) \tag{2b}$$

$$\mathbf{\Gamma}_m = \chi_a (\mathbf{n} \cdot \mathbf{H}) \mathbf{n} \times \mathbf{H} \tag{2c}$$

where:

$$\gamma_1 = \alpha_3 - \alpha_2, \qquad \gamma_2 = \alpha_2 + \alpha_3. \tag{3a,b}$$

The viscosities α_2 and α_3 are two of the six Leslie viscosities. The term $\delta f_d / \delta \mathbf{n}$ denotes the functional derivative of the distortion free energy density f_d with respect to the director $\mathbf{n}$, χ_a is the magnetic susceptibility anisotropy, and $\mathbf{H}$ is the magnetic field. The kinematic quantities appearing in the constitutive equations are defined as follow:

$$\mathbf{N} = \dot{\mathbf{n}} - \mathbf{\Omega} \cdot \mathbf{n} \tag{4a}$$

$$\mathbf{\Omega} = \frac{1}{2}[(\nabla \mathbf{V})^T - \nabla \mathbf{V}] \tag{4b}$$

$$\mathbf{A} = \frac{1}{2}[(\nabla \mathbf{V})^T + \nabla \mathbf{V}] \tag{4c}$$

where $\mathbf{V}$ is the velocity, $\mathbf{N}$ is the angular velocity of the director relative to that of the fluid, $\mathbf{\Omega}$ is the vorticity tensor, and $\mathbf{A}$ is the rate of deformation tensor. The superposed dot denotes the material time derivative.

The total free energy is expressed as follows [22]:

$$F = \int_V f_d \, dV + \int_V f_m \, dV + \int_S f_s \, dS \tag{5}$$

where f_d, f_m and f_s are the distortion, magnetic and surface free energy densities, respectively, and are defined as follow [22, 23]:

$$f_d = \frac{1}{2} K_{11} (\nabla \cdot \mathbf{n})^2 + \frac{1}{2} K_{22} (\mathbf{n} \cdot \nabla \times \mathbf{n})^2 + \frac{1}{2} K_{33} \| \mathbf{n} \times \nabla \times \mathbf{n} \|^2 \tag{6a}$$

$$f_m = -\frac{1}{2} \chi_a (\mathbf{n} \cdot \mathbf{H})^2 \tag{6b}$$

$$f_s = \frac{1}{2} W_o \sin^2 (\phi - \phi_o). \tag{6c}$$

K_{11}, K_{22} and K_{33} are the splay, twist and bend elastic constants, respectively. W_o is the surface anchoring strength, and ϕ and ϕ_o are the actual and preferred anchoring angles at the droplet surface, respectively. In nematic bipolar droplets, the director is anchored tangentially to the surface; consequently, $W_o \to \infty$ and $\phi = \phi_o$ in equation (6*c*) and there is no surface contribution to the total free energy. Chan and Rey [10] accounted for the surface free energy in their numerical study of spherical bipolar droplets by using finite values for W_o, which allows the director to rotate on the surface.

2.2. *Governing equations and auxiliary conditions*

Figure 1 shows the cross-sections of a spherical bipolar droplet and an elongated bipolar droplet, and defines the cylindrical coordinate system. ϕ is the polar angle measured from the z-axis. Since bipolar droplets have axisymmetry, this study is restricted to a two-dimensional examination of the magnetically-induced director reorientation dynamics inside a circle of radius R with area $A_c = \pi R^2$ and in ellipses with minor axis length a, major axis length b, aspect ratio $c = b/a$ and area $A_e = \pi ab$. Furthermore, this study is restricted to

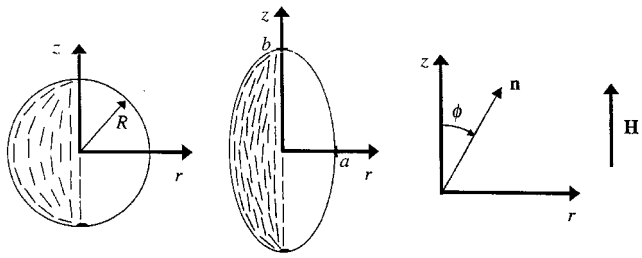

Figure 1. Schematic representation of the cross section of a spherical droplet (represented by a circle) and an elongated droplet (represented by an ellipse), and definition of the cylindrical coordinate system. The z-axis is along the axis of symmetry, which is the line joining the two point defects. R is the circle radius, a and b are the minor and major axis lengths of the ellipse, ϕ is the polar angle, $\mathbf{n}$ is the director and $\mathbf{H}$ is the magnetic field.

the cases where $A_e = A_c$. This means that all cross-sectional areas are the same, implying that the results apply to spherical and elongated droplets that have the same volume. In addition, the magnetic field is parallel to the z-axis; i.e.

$$\mathbf{H} = (0, 0, H) \tag{7}$$

It is assumed that the characteristic times of the velocity variations are much shorter than those of the director; i.e. the velocity follows the director instantaneously [24]. Consequently, backflow effects are minimal and neglected. The transient planar two-dimensional director field is defined as follows:

$$\mathbf{n}(r, z, t) = (\sin\phi(r, z, t), 0, \cos\phi(r, z, t)) \tag{8}$$

where the unit length constraint, $\mathbf{n}\ \mathbf{n} = 1$, is automatically satisfied.

The equation that governs the behaviour of ϕ is the θ-component of the torque balance (see equation (1)). The following scaling relations are used to non-dimensionalize the governing equation:

$$K^*_{ii} = \frac{K_{ii}}{K} \text{ (for } i = 1, 2, 3) \quad \text{where} \quad K = \frac{K_{11} + K_{33}}{2} \tag{9a}$$

$$r^* = \frac{r}{R}, \quad z^* = \frac{z}{R}, \quad a^* = \frac{a}{R} \quad \text{and} \quad b^* = \frac{b}{R} \tag{9b}$$

$$t^* = \frac{tK}{\gamma_1 R^2} \tag{9c}$$

$$Z_o = \frac{\chi_a H^2 R^2}{K}. \tag{9d}$$

The dimensionless Zocher number Z_o gives the relative magnitude of magnetic to elastic torques. The superscript asterisks denote dimensionless variables. By incorporating equations (1) to (9), the following dimensionless, time-dependent, second order, two-dimensional, nonlinear partial differential equation is obtained to describe the magnetically-induced director reorientation dynamics:

$$\frac{\partial\phi}{\partial t^*} = \kappa_1 + \kappa_2\frac{\partial\phi}{\partial r^*} + \kappa_3\frac{\partial\phi}{\partial r^*}\frac{\partial\phi}{\partial r^*} + \kappa_4\frac{\partial^2\phi}{\partial r^{*2}} + \kappa_5\frac{\partial\phi}{\partial z^*} + \kappa_6\frac{\partial\phi}{\partial z^*}\frac{\partial\phi}{\partial z^*} + \kappa_7\frac{\partial^2\phi}{\partial z^{*2}} + \kappa_8\frac{\partial\phi}{\partial r^*}\frac{\partial\phi}{\partial z^*} + \kappa_9\frac{\partial^2\phi}{\partial r^*\partial z^*} - \frac{1}{2}Z_o\sin(2\phi) \tag{10}$$

where the spatially- and angle-dependent elastic functions $\{\kappa_i\}$, $i = 1, \ldots 9$, are given in the Appendix.

The dimensionless total free energy is obtained by combining equations (5) to (9). It is expressed as follows:

$$F^* = F^*_d + F^*_m + F^*_s \tag{11}$$

where

$$F^*_d = 2\pi\iint\left(\kappa_{10} + \kappa_{11}\frac{\partial\phi}{\partial r^*} + \kappa_{12}\frac{\partial\phi}{\partial z^*} + \kappa_{13}\frac{\partial\phi}{\partial r^*}\frac{\partial\phi}{\partial r^*} + \kappa_{14}\frac{\partial\phi}{\partial r^*}\frac{\partial\phi}{\partial z^*} + \kappa_{15}\frac{\partial\phi}{\partial z^*}\frac{\partial\phi}{\partial z^*}\right)dr^*\,dz^* \tag{12a}$$

$$F^*_m = -\pi Z_o\iint r^*\cos^2\phi\,dr^*\,dz^*. \tag{12b}$$

The spatially and angle dependent elastic functions $\{\kappa_i\}$, $i = 10, \ldots, 15$, are listed in the Appendix. Note that F^*_s is not given since it does not contribute to the total free energy when the director is anchored along the easy axis direction at the droplet surface, which is the case studied in this paper.

As mentioned above, there is symmetry about the z-axis in bipolar droplets, and equation (10) can be solved numerically within only the half-circle or half-ellipse where $r^* \geqslant 0$ (see figure 1). Consequently, the initial and boundary conditions are as follow:

$$\phi = \phi_o(r^*, z^*) \quad \text{at} \quad t^* = 0, \quad r^* \geqslant 0, \quad -1 \leqslant z^* \leqslant 1 \tag{13a}$$

$$\frac{\partial\phi}{\partial r^*} = 0 \quad \text{at} \quad t^* \geqslant 0, \quad r^* = 0, \quad -1 \leqslant z^* \leqslant 1 \tag{13b}$$

$$\phi = -\tan^{-1}\left(\frac{z^*}{r^*}\right) \quad \text{at} \quad t^* \geqslant 0, \quad r^* > 0, \quad z^* = (b^{*2} - c^2 r^{*2})^{1/2}. \tag{13c}$$

2.3. *Numerical method of solution*

The Galerkin finite element method [25], with bilinear basis functions and 200 elements, is used for the numerical solution. A set of nonlinear, time-dependent,

Table 1. Scaled physical constants used in the present work; see text for definitions.

Constant	Values					
K_{11}^*	0.6667					
K_{33}^*	1.3333					
c	1.0	1.1	1.2	1.3	1.4	1.5
	1.6	1.7	1.8	1.9	2.0	2.1
	2.2	2.3	2.4	2.5		
Z_o	0	25	50	100	200	300
	400	500	600	700	800	900
	1000	1100	1200	1300	1400	1500
	1600	1700	1800	1900	2000	

ordinary differential equations are obtained after spatial discretization, which are solved simultaneously using a Newton–Raphson iteration scheme. Convergence is assumed when the length of the vector of the difference between two successive computer solution vectors is less than 10^{-6}. A finite difference method is used to discretize time, and a first order implicit Euler predictor-corrector method is used for time integration. To minimize the computing time without losing accuracy, an adaptive time step control scheme [26] is used. This method takes into account the local truncation error and a user-specified tolerance; the main idea is that large (small) time steps are taken when little (significant) changes occur in the transient solution. It is noted that this method of solution is applicable to any arbitrary geometry, such as the circular and elliptical geometries studied in this paper.

The dependent variable is ϕ, and the independent variables are (r^*, z^*, t^*). The parameters are the dimensionless splay K_{11}^* and bend K_{33}^* elastic constants, dimensionless Zocher number Z_o, and aspect ratio c. Although a comprehensive parametric study was performed on these parameters, the restricted number of simulation results presented here (see table 1) best reflect the objectives of this paper (see § 1). The values for the parameters K_{11}^*, K_{33}^*, c and Z_o listed in table 1 are typical of PDLC films. Moreover, the scaling of time is appropriate to the present system. This can be checked by substituting the typical parameter values listed in table 2 and obtain $Z_o = 3.38$ and $t^* = 0.12$–1.2. In addition, it must be noted that the values chosen for K_{11}^* and K_{33}^* satisfy the $(K_{33}/K_{11}) > 1$ criterion to form a bipolar droplet [16], and that director reorientation dynamics can occur for $Z_o > 3.38$ (see table 1).

Table 2. Parameter values; see text for definitions.

Parameter	Value	References
$K/10^{-11}$ N	1	[16]
$\gamma_1/10^{-3}$ Pa s	81	[24]
$\chi_a/\mathrm{N\,T^{-2}\,m^{-2}}$	1.353	[24]
$R/10^{-6}$ m	1	[12, 16]
H/T	5	[13]
$t/10^{-3}$ s	1–10	[12, 13, 16]

3. Results and discussion

This section presents numerical results obtained from the solution of the model outlined above, and is divided into three parts. The first part defines a mean magnitude of the orientation angle that can be computed using the numerical results, and shows how this angle can be related to PDLC light transmittance experimental results found in the literature. The second part presents results from simulations representing the on-state; i.e. when a magnetic field is applied to a droplet. On the other hand, the third part presents numerical results from simulations representing the off-state; i.e. when the magnetic field is removed from a droplet after the steady state director configuration has been achieved during the on-state. Furthermore, comparison of these numerical results with experimental data found in the literature for the on- and off-states is made, to validate the model presented in § 2.2.

3.1. *Mean orientation angle*

A mean magnitude of the orientation angle can be obtained using the following definition:

$$\langle \| \phi \| \rangle = \frac{1}{\pi} \int_{-1}^{1} \int_{r_l^*}^{r_u^*} |\phi| \, \mathrm{d}r^* \, \mathrm{d}z^* \qquad (14\,a)$$

where:

$$r_l^* = -\left(a^{*2} - \frac{z^{*2}}{c^2}\right)^{1/2} \quad \text{and} \quad r_u^* = \left(a^{*2} - \frac{z^{*2}}{c^2}\right)^{1/2}. \qquad (14\,b)$$

$\langle \| \phi \| \rangle$ is used in this paper to relate droplet director configurations to light scattering and transmittance in PDLC films. The directors become more aligned with

the axis of symmetry as $\langle \| \phi \| \rangle$ decreases (see figure 1 for definition of ϕ). In the limit of $\langle \| \phi \| \rangle = 0$, all the directors are aligned with the axis of symmetry.

Several special cases of $\langle \| \phi \| \rangle$ are used in this paper. $\langle \| \phi_{ss} \| \rangle$ denotes the steady state values of $\langle \| \phi \| \rangle$ in the on- and off-states. $\langle \| \phi_o \| \rangle$ represents the mean magnitude of the orientation angle before the magnetic field is turned on; this means that $\langle \| \phi_o \| \rangle$ also corresponds to the steady state value of $\langle \| \phi \| \rangle$ in the off-state (see § 3.2). Moreover, $\langle \| \phi_o \| \rangle$ also corresponds to the maximum value $\langle \| \phi \| \rangle$ can have for a given aspect ratio c. Consequently, $\langle \| \phi \| \rangle_{max} = \langle \| \phi_o \| \rangle$. Lastly, the minimum value $\langle \| \phi \| \rangle$ can have for a given aspect ratio c is denoted as $\langle \| \phi \| \rangle_{min}$ and this occurs at steady state in the on-state for $Z_o \to \infty$, where maximum reorientation occurs. However, as will be shown below, $Z_o = 2000$ is sufficient to provide maximum reorientation (see figure 6) and will be used in this paper to obtain $\langle \| \phi \| \rangle_{min}$.

In general, light scattering depends on the director configuration within a droplet. Wu *et al.* [11] presented a simple but useful approach to relate the liquid crystal refractive indices to the bipolar configurations, which can be used to explain light transmittance in PDLC films. Although this approach is not rigorous, it does reflect current understanding on this complex optical phenomenon. In addition, as will be shown below, although the results are from a single droplet and not from a sample of droplets as in a PDLC film, the numerical results and analyses are consistent with experimental data on PDLC light transmittance. Drzaic [3] has already used the fact that the optical phenomenon of a PDLC film can be explained by looking at individual droplets. According to Wu *et al.* [11], the average ordinary refractive index $\langle n_o \rangle$ of a bipolar droplet in the absence of an external field is greater than the ordinary refractive index n_o for a uniform director configuration that is unconfined. Hence, light is scattered and the PDLC film appears opaque since $\langle n_o \rangle > n_o = n_p$, where n_p is the polymer refractive index. This corresponds to the case where $\langle \| \phi \| \rangle$ is at a finite value. As the bulk director configuration becomes more uniform from the effect of the external field, $\langle \| \phi \| \rangle$ decreases and $\langle n_o \rangle$ approaches $n_o = n_p$. This means that light is less scattered and the PDLC film appears more transparent. In the limit where all the directors are aligned along the axis of symmetry (i.e., $\langle \| \phi \| \rangle = 0$), $\langle n_o \rangle = n_o = n_p$, light is not scattered by the bipolar droplet and the PDLC film appears transparent. Therefore, light transmittance is inversely related to $\langle \| \phi \| \rangle$.

3.2. *On-state dynamics*

Figure 2 is a plot of the mean magnitude of the orientation angle $\langle \| \phi \| \rangle$ versus dimensionless time t^* for Zocher number $Z_o = 2000$ and at the following aspect ratios: $c = 1.0$ (solid line), $c = 1.5$ (long dashed line) and $c = 2.0$ (short dashed line). As mentioned in § 3.1, a value of $Z_o = 2000$ is used to achieve maximum director reorientation and $\langle \| \phi \| \rangle_{min}$. This figure is representative of simulations obtained using other c values and shows that for any Zocher number: (a) in the on-state $\langle \| \phi \| \rangle$ decreases exponentially from $\langle \| \phi_o \| \rangle$ and eventually saturates at a steady state value $\langle \| \phi_{ss} \| \rangle$, and (b) in the off-state $\langle \| \phi \| \rangle$ increases exponentially from the steady state value obtained in the on-state and eventually saturates at the initial value $\langle \| \phi_o \| \rangle$. The same dynamic response is obtained for the on- and off-states as the magnetic field is turned on ($Z_o = 2000$) and off ($Z_o = 0$) repeatedly, as is typically done in PDLC film operation. Figure 2 provides an explanation for the typical experimental plot of light transmittance versus time, upon application and followed by removal of an external field [15]. In the on-state, the light transmittance increases exponentially at early times but then saturates at later times. Once the field is turned off, however, the light transmittance decreases exponentially and then saturates with time. As discussed in § 3.1, light scattering and transmittance depends on the director configuration within the droplets. Consequently, the exponential increase in light transmittance during the on-state at early times is due to the exponential decrease in $\langle \| \phi \| \rangle$. Moreover, the saturation in light transmittance at later times is due to the director configuration reaching steady state which also corresponds to an equilibrium state. Similarly,

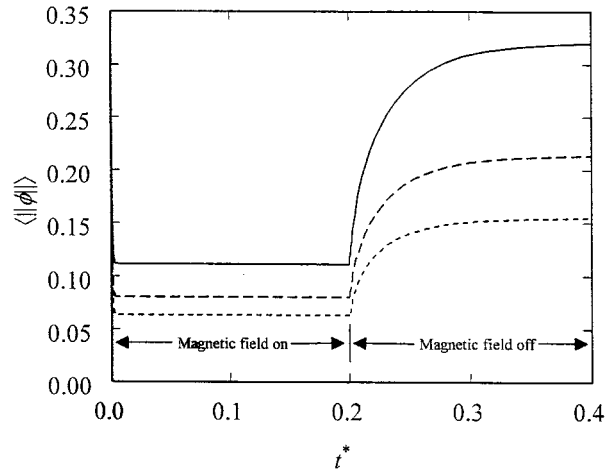

Figure 2. Mean magnitude of the orientation angle $\langle \| \phi \| \rangle$ versus dimensionless time t^* for Zocher number $Z_o = 2000$ and at the following aspect ratios: $c = 1.0$ (solid line), $c = 1.5$ (long dashed line) and $c = 2.0$ (short dashed line). The magnetic field is on during the time range $0 \leqslant t^* < 0.2$, but is off during the time range $0.2 < t^* \leqslant 0.4$. The same curves are obtained when the magnetic field is turned on and off repeatedly.

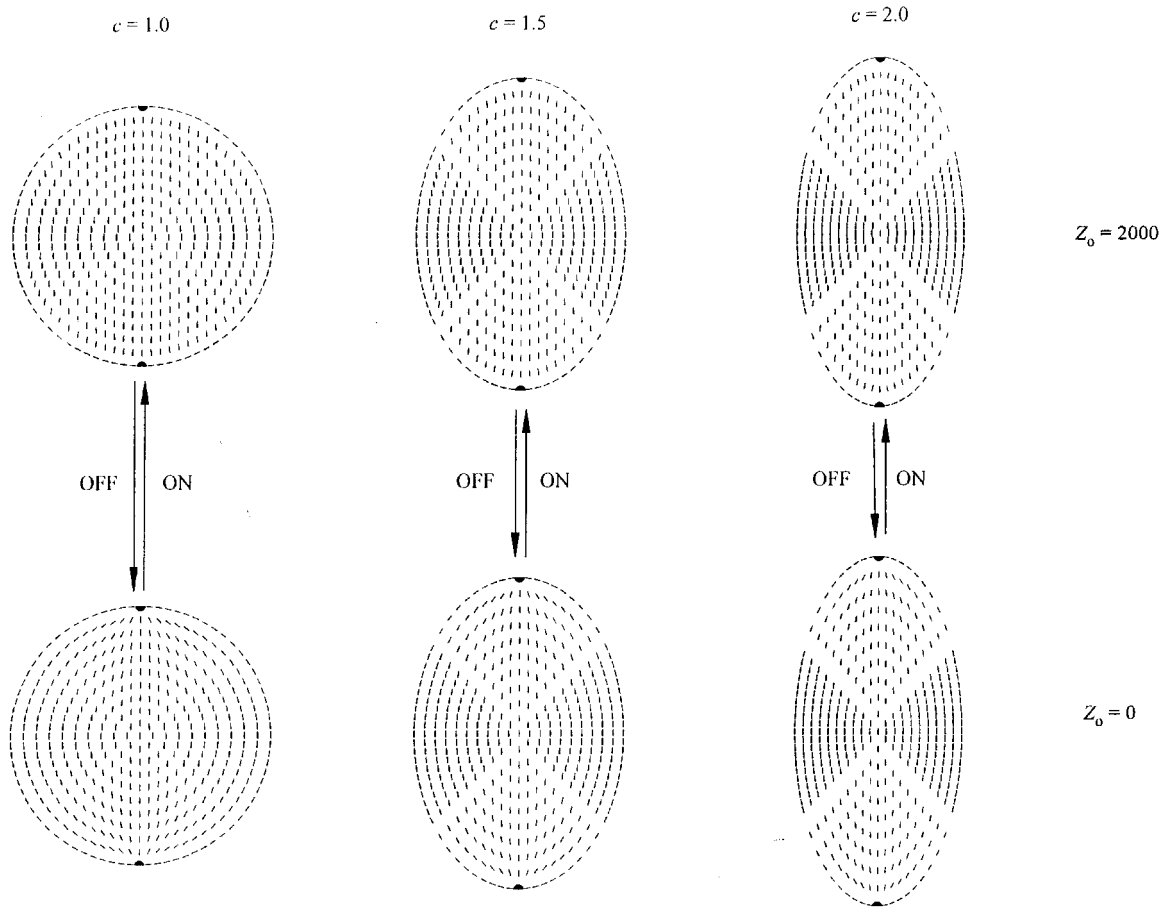

Figure 3. Steady state director configurations in bipolar droplets with aspect ratios $c = 1.0$ (left column), $c = 1.5$ (middle column) and $c = 2.0$ (right column) in the off-state ($Z_o = 0$, bottom row) and on-state ($Z_o = 2000$, top row). The arrows indicate that the configurations are reversible as the field is turned on and off repeatedly as in PDLC film operation.

the exponential decrease and saturation in light transmittance in the off-state is due to the exponential increase and saturation in $\langle \| \phi \| \rangle$ during the off-state, as shown in figure 2.

Figure 3 shows the steady state director configurations in droplets with aspect ratios $c = 1.0$ (left column), $c = 1.5$ (middle column) and $c = 2.0$ (right column) in the off-state ($Z_o = 0$, bottom row) and on-state ($Z_o = 2000$, top row). These configurations are representative of other simulations using different c and Z_o values, and show that: (a) the same director configurations are obtained when the magnetic field is turned on and off repeatedly for a given droplet, (b) the steady state director configurations are very similar between droplets, and (c) because of (a) and (b) all would be useful for PDLC film operation. Consequently, as discussed below, other criteria must be employed to evaluate the effect of c on PDLC film performance.

Figure 4 is a plot of the maximum value $\langle \| \phi \| \rangle_{max}$ (squares) and minimum value $\langle \| \phi \| \rangle_{min}$ (triangles) of the

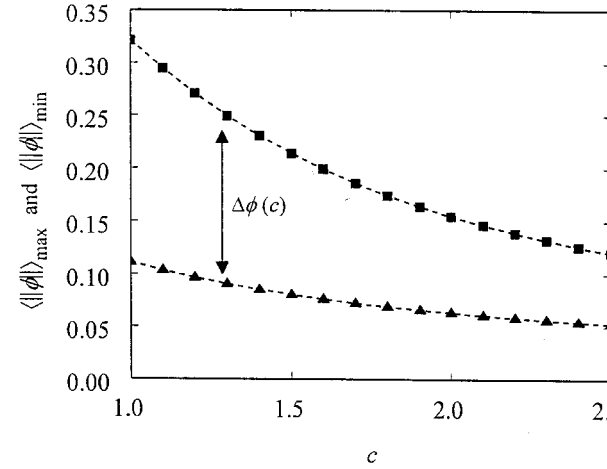

Figure 4. Maximum value $\langle \| \phi \| \rangle_{max}$ (squares) and minimum value $\langle \| \phi \| \rangle_{min}$ (triangles) of the mean magnitude of the orientation angle versus aspect ratio c. $\Delta\phi$ represents the difference between $\langle \| \phi \| \rangle_{max}$ and $\langle \| \phi \| \rangle_{min}$ for any given aspect ratio c.

mean magnitude of the orientation angle versus aspect ratio c. This figure indicates that $\langle \| \phi \| \rangle_{max}$ and $\langle \| \phi \| \rangle_{min}$ decrease as c increases. This can be explained by looking at the droplet director distortion. As shown in figure 3, the director configuration becomes less distorted (i.e. $\langle \| \phi \| \rangle$ decreases) when the droplet shape goes from spherical ($c = 1$) to elongated ($c > 1$). In addition $\Delta\phi = \langle \| \phi \| \rangle_{max} - \langle \| \phi \| \rangle_{min}$ also decreases with c for the same reason, that there is less director distortion as c increases. Thus the directors are required to reorient less in the on-state as the droplet shape becomes more elongated and $\Delta\phi$ decreases. In relation to PDLC films, figure 4 indicates that spherical or slightly elongated droplets ($c \cong 1$) are preferred because they have higher values of $\Delta\phi$, translating into higher light contrast between the on- and off-states. This is a requirement for efficient operation of a PDLC film.

The switching field strength is an important parameter in PDLC film operation. It is defined as the electric or magnetic field required to reach 90% light transmittance in the on-state [16]. In this paper, the switching field strength is denoted as $Z_{o,90}$ and is defined as the field required to make the director reorient from $\langle \| \phi_o \| \rangle$ to $[\langle \| \phi_o \| \rangle - 0.9\Delta\phi]$. Figure 5 shows the relationship between $Z_{o,90}$ and aspect ratio c. This figure clearly indicates that $Z_{o,90}$ increases with c, which is consistent with experimental observations [3]. This can be explained using figure 6, which is a plot of $\langle \| \phi_{ss} \| \rangle$ versus Z_o for the following aspect ratios: $c = 1.0$ (circles), $c = 1.5$ (squares), $c = 2.0$ (triangles) and $c = 2.5$ (diamonds). A solid line is superimposed onto the exponential curves and represents $Z_{o,90}$ for different c values. This solid line indicates that $Z_{o,90}$ increases with c; in other words, the required switching field strength increases as the droplets become more elongated. In terms of PDLC film operation, spherical or slightly elongated droplets ($c \cong 1$) are preferred because they require lower switching field strengths.

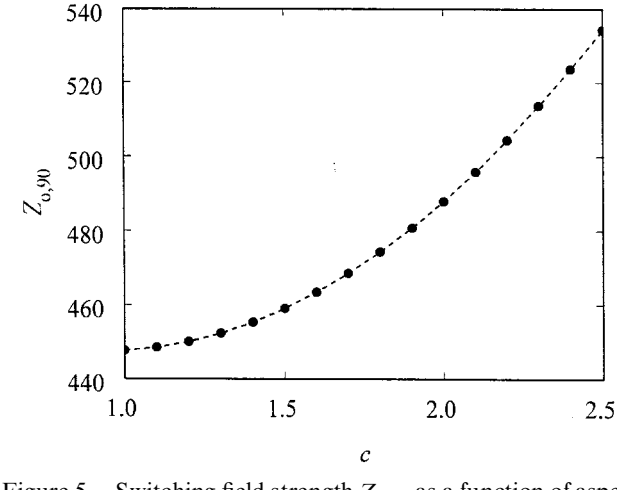

Figure 5. Switching field strength $Z_{o,90}$ as a function of aspect ratio c. The switching field strength increases with aspect ratio, which is consistent with experimental observations found in the literature.

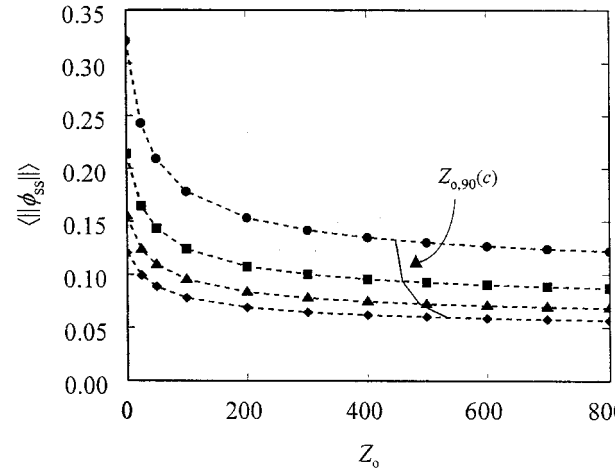

Figure 6. Mean magnitude of the orientation angle at steady state $\langle \| \phi_{ss} \| \rangle$ versus Zocher number Z_o for the following aspect ratios: $c = 1.0$ (circles), $c = 1.5$ (squares), $c = 2.0$ (triangles) and $c = 2.5$ (diamonds). The superimposed solid line represents the switching field strength $Z_{o,90}$ as a function of c. Consistent with figure 5, $Z_{o,90}$ increases with c.

In summary, spherical or slightly elongated droplets ($c \cong 1$) are preferred for PDLC film operation because they provide better light contrast between the on- and off-states and require lower switching fields.

3.3. *Off-state dynamics*

Efficient PDLC film operation requires a short decay time [3, 4], which is defined as the time required for light transmittance to decrease to 10% light transmittance after the external field is turned off [16]. In this paper, the decay time is denoted as t_d and is defined as the time required for $\langle \| \phi \| \rangle$ to go from $\langle \| \phi_{ss} \| \rangle$ in the on-state to $(\langle \| \phi_o \| \rangle + 0.1\Delta_{ss})$, where $\Delta_{ss} = \langle \| \phi_{ss} \| \rangle - \langle \| \phi_o \| \rangle$. The decay time t_d is plotted against the aspect ratio c in figure 7 for the case of $Z_o = 2000$ (which gives the maximum possible reorientation) in the on-state. This figure clearly shows that t_d decreases as c increases, which is consistent with experimental observations [3, 4]. This is because the directors do not have to reorient much for $c \cong 2.5$ (small Δ_{ss} in general for any Z_o value and small $\Delta\phi$ in particular for $Z_o = 2000$), but requires to reorient significantly for $c \cong 1$ (large Δ_{ss} in general for any Z_o value and large $\Delta\phi$ in particular for $Z_o = 2000$), such as shown in figures 3 and 4 for $Z_o = 2000$. This is unlike the relaxation of stored elastic free energy explanation offered by Drzaic and Muller [3, 4] for this phenomenon. One difference between the work by Drzaic and Muller

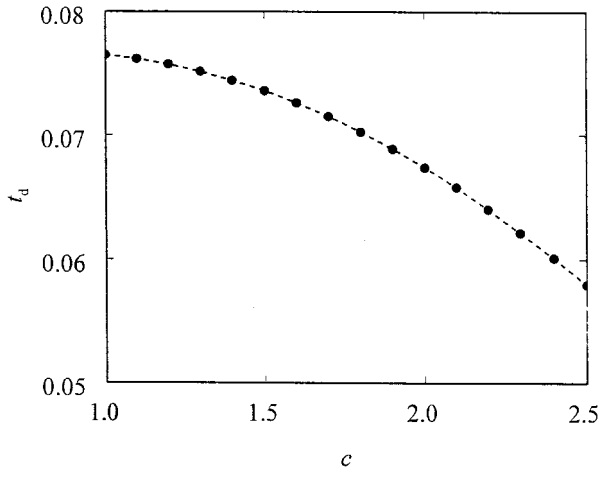

Figure 7. Decay time t_d as a function of aspect ratio c for the case of Zocher number $Z_o = 2000$, which induces maximum director reorientation in the on-state. Consistent with published experimental data, t_d decreases as c increases.

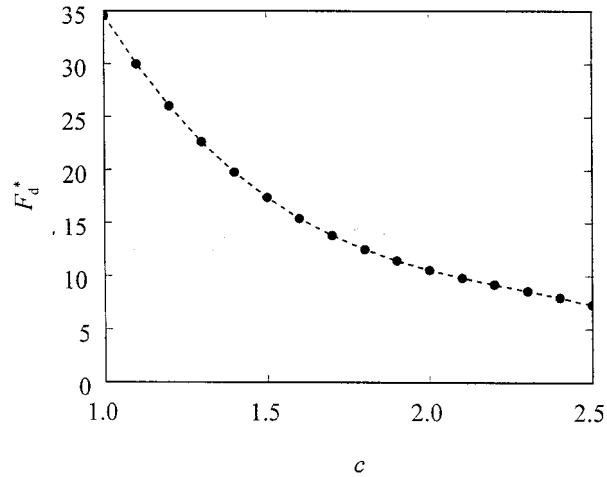

Figure 8. Dimensionless total stored distortion free energy F_d^* versus aspect ratio c at steady state for the case of Zocher number $Z_o = 2000$. The director configuration becomes less distorted as the droplet becomes more elongated (see figure 1), and this decreases F_d^*.

and the work presented in this paper is the orientation of the droplet. In this paper the droplet is oriented with the axis of symmetry aligned with the field direction; however, the experimental results obtained by Drzaic and Muller [3, 4] were from PDLC films containing significantly large numbers of droplets with their axis of symmetry oriented randomly. Furthermore, our numerical results for the stored distortion (or elastic) free energy and its relaxation rate are the reverse of the results of Drzaic and Muller. They concluded that the stored distortion free energy is higher in an elongated droplet than in a spherical one, and it is this higher free energy that drives director relaxation in the off-state and gives elongated droplets shorter decay times.

Figure 8 is a plot of the dimensionless total stored distortion free energy F_d^* versus aspect ratio c at steady state for the case of $Z_o = 2000$. Figure 9 is a plot of the rate of change of the dimensionless total stored distortion free energy in the off-state, corresponding to figure 8, and for the following aspect ratios: $c = 1.0$ (circles), $c = 1.5$ (squares), $c = 2.0$ (triangles) and $c = 2.5$ (diamonds). Figure 9 is consistent with figure 8; i.e. the initial relaxation rate of stored distortion free energy is greater (lower) for a droplet with higher (lower) stored distortion free energy. Consequently, for bipolar elongated droplets with the magnetic field applied along the axis of symmetry, the decay time depends primarily on the value of Δ_{SS}. The stored distortion free energy may play a secondary role, however.

Another point to note from figure 7 is that eventually the t_d versus c curve will intersect the c axis as c increases to $c \cong 2.75$. This case corresponds to a very elongated droplet where most if not all of the directors are aligned with the axis of symmetry. Consequently, there will be

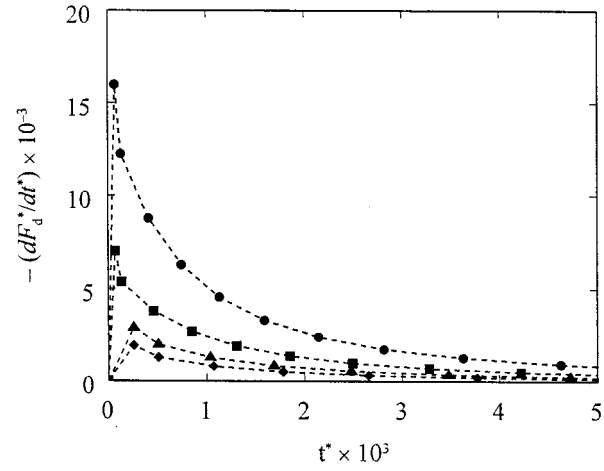

Figure 9. Rate of change of the dimensionless total stored distortion free energy dF_d^*/dt^* in the off-state for the following aspect ratios: $c = 1.0$ (circles), $c = 1.5$ (squares), $c = 2.0$ (triangles) and $c = 2.5$ (diamonds). Figure 9 is consistent with figure 8; i.e. the initial relaxation rate of F_d^* is greater (lower) for a droplet with higher (lower) stored distortion free energy.

no director reorientation upon application of external field and no decay time will be exhibited in the off-state. In addition, very elongated droplets ($c \geqslant 2.75$) require very high switching field strengths (see figure 5) and will not provide good contrast (see figure 4). Consequently, very elongated droplets ($c \geqslant 2.75$) are not recommended for PDLC film operation.

In summary, in terms of decay time, elongated droplets ($c \cong 2.5$) are preferred for PDLC film operation since they have shorter decay times.

4. Conclusions

Numerical results from the solution of the Leslie–Ericksen continuum theory to describe the magnetically-induced nematic director reorientation dynamics inside ellipses have been presented in this paper. These numerical results apply to elongated bipolar droplets with the magnetic field applied along the axis of symmetry direction. The effect of droplet shape has been elucidated by varying the aspect ratio of the ellipse. In the limit where the aspect ratio is unity, the ellipse becomes a circle which corresponds to a spherical droplet.

The numerical results replicate frequently-reported experimental observations on the performance of PDLC films. These observations are the following: (a) the light transmittance increases exponentially at first but then saturates as the external applied field increases, (b) the light transmittance increases exponentially initially but then saturates with time in the on-state, (c) the light transmittance decreases exponentially initially but then saturates with time in the off-state, (d) the switching field strength increases as the droplet becomes more elongated, and (e) the decay time decreases as the droplets become more elongated. These numerical results suggest that spherical or slightly elongated droplets are preferred for PDLC film operation because they provide better light contrast between the on- and off-states and require lower switching field strengths, even though their decay times are longer.

The author gratefully acknowledges financial support from Ryerson Polytechnic University and the Natural Sciences and Engineering Research Council of Canada.

Appendix

The elastic functions $\{\kappa_i\}$, $i = 1, \ldots, 15$, in equations (10) and (12 *a*) are defined as follows:

$$\kappa_1 = -\frac{1}{2}\frac{1}{r^{*2}}K_{11}^{*}\sin(2\phi) \tag{A1}$$

$$\kappa_2 = \frac{1}{r^{*}}(K_{11}^{*}\cos^2\phi + K_{33}^{*}\sin^2\phi) \tag{A2}$$

$$\kappa_3 = \frac{1}{2}(K_{33}^{*} - K_{11}^{*})\sin(2\phi) \tag{A3}$$

$$\kappa_4 = K_{11}^{*}\cos^2\phi + K_{33}^{*}\sin^2\phi \tag{A4}$$

$$\kappa_5 = \frac{1}{2}\frac{1}{r^{*}}(K_{33}^{*} - K_{11}^{*})\sin(2\phi) \tag{A5}$$

$$\kappa_6 = \frac{1}{2}(K_{11}^{*} - K_{33}^{*})\sin(2\phi) \tag{A6}$$

$$\kappa_7 = K_{11}^{*}\sin^2\phi + K_{33}^{*}\cos^2\phi \tag{A7}$$

$$\kappa_8 = (K_{33}^{*} - K_{11}^{*})\cos(2\phi) \tag{A8}$$

$$\kappa_9 = (K_{33}^{*} - K_{11}^{*})\sin(2\phi) \tag{A9}$$

$$\kappa_{10} = \frac{1}{2}\frac{1}{r^{*}}K_{11}^{*}\sin^2\phi \tag{A10}$$

$$\kappa_{11} = \frac{1}{2}K_{11}^{*}\sin(2\phi) \tag{A11}$$

$$\kappa_{12} = -K_{11}^{*}\sin^2\phi \tag{A12}$$

$$\kappa_{13} = \frac{1}{2}r^{*}(K_{11}^{*}\cos^2\phi + K_{33}^{*}\sin^2\phi) \tag{A13}$$

$$\kappa_{14} = \frac{1}{2}r^{*}(K_{33}^{*} - K_{11}^{*})\sin(2\phi) \tag{A14}$$

$$\kappa_{15} = \frac{1}{2}r^{*}(K_{11}^{*}\sin^2\phi + K_{33}^{*}\cos^2\phi). \tag{A15}$$

References

[1] Dubois-Violette, E., and Parodi, O., 1969, *J. Phys. (Paris) Colloq.*, **30,** C4-57.

[2] Candau, S., Le Roy, P., and Debeauvais, F., 1973, *Mol. Cryst. liq. Cryst.*, **23,** 283.

[3] Drzaic, P. S., 1988, *Liq. Cryst.*, **3,** 1543.

[4] Drzaic, P. S., and Muller, A., 1989, *Liq. Cryst.*, **5,** 1467.

[5] Wu, B.-G., Erdmann, J. H., and Doane, J. W., 1989, *Liq. Cryst.*, **5,** 1453.

[6] Vilfan, I., Vilfan, M., and Zumer, S., 1989, *Phys. Rev. A*, **40,** 4724.

[7] Jain, S. C., and Rout, D. K., 1991, *J. appl. Phys.*, **70,** 6988.

[8] Huang, W., and Tuthill, G. F., 1994, *Phys. Rev. E*, **49,** 570.

[9] Ding, J., Zhang, H., Lu, J., and Yang, Y., 1995, *Jpn. J. appl. Phys.*, **34,** 1928.

[10] Chan, P. K., and Rey, A. D., 1997, *Liq. Cryst.*, **23,** 677.

[11] Wu, B.-G., West, J. L., and Doane, J. W., 1987, *J. appl. Phys.*, **62,** 3925.

[12] Doane, J. W., 1990, *Liquid Crystals: Applications and Uses*, Vol. 1, edited by B. Bahadur (World Scientific), pp. 361–395.

[13] Li, Z., Kelly, J. R., Palffy-Muhoray, P., and Rosenblatt, C., 1992, *Appl. Phys. Lett.*, **60,** 3132.

[14] Erdmann, J. H., Lackner, A. M., Sherman, E., and Margerum, J. D., 1993, *J. SID*, **1,** 57.

[15] Montgomery, G. P., Smith, G. W., and Vaz, N. A., 1994, *Liquid Crystalline and Mesomorphic Polymers*, edited by V. P. Shibaev and L. Lam (Springer-Verlag), pp. 149–192.

[16] Drzaic, P. S., 1995, *Liquid Crystal Dispersions* (World Scientific).

[17] Chan, P. K., and Rey, A. D., 1995, *Comput. Mater. Sci.*, **3,** 377.

[18] Chan, P. K., and Rey, A. D., 1995, *Macromol. Theory Simul.*, **4,** 873.

[19] Chan, P. K., and Rey, A. D., 1996, *Macromolecules*, **29,** 8934.

[20] Chan, P. K., and Rey, A. D., 1997, *Macromolecules*, **30,** 2135.

[21] Chan, P. K., 1998, *Recent Res. Devel. Macromol. Res.*, **3,** 439.
[22] De Gennes, P. G., and Prost, J., 1993, *The Physics of Liquid Crystals*, 2nd Edn (Clarendon Press).
[23] Rapini, A., and Papoular, M. J., 1969, *J. Phys. (Paris) Colloq.*, **30,** C4-54.
[24] Blinov, L. M., and Chigrinov, V. G., 1994, *Electrooptic Effects in Liquid Crystalline Materials* (Springer), Chap. 4.
[25] Fletcher, C. A. J., 1984, *Computational Galerkin Methods* (Springer).
[26] Finlayson, B. A., 1980, *Nonlinear Analysis in Chemical Engineering* (McGraw-Hill).